61^{st} CONGRESS OF ISTAM

Section code : Solid Mechanics

Poly - FEM for the analysis of plane elasticity problems

Piska Raghu[1], Amirtham Rajagopal[1], and Balaji Kasi[1]

[1]Department of Civil Engineering, Indian Institute of Technology Hyderabad, Telangana, India.

Abstract

In this work we present polygonal finite element method (Poly-FEM) for the analysis of two dimensional plane elasticity problems. The generation of meshes consisting of $n-$ sided polygonal finite elements is based on the generation of a centroidal Voronoi tessellation (CVT). An unstructured tessellation of a scattered point set, that minimally covers the proximal space around each point in the point set is generated whereby the method also includes tessellation of non-convex domains.In this work, a patch recovery type of stress smoothing technique that utilizes polygonal element patches for obtaining smooth stresses is proposed for obtaining the smoothed finite element stresses. A recovery type $a - posteriori$ error estimator that estimates the energy norm of the error from the recovered solution is then adopted for the polygonal finite element method. The refinement of the polygonal elements is then made on an region by region basis through a refinement index. For the numerical integration of the Galerkin weak form over polygonal finite element domains we resort to classical Gaussian quadrature applied to triangular sub domains of each polygonal element.

Introduction

The finite element method is a powerful numerical tool for solving partial differential equations. The use of two dimensional triangular or quadrilateral elements and three dimensional tetrahedral or hexahedral elements is the popular standard case. However, there are associated complexities such as developing robust and fast algorithms for generating quality meshes on two or three dimensional complex geometries of micro structures, distortion effects under large deformation, complexities in development and use of higher order elements and the need for efficient quadrature schemes for the evaluation of integrals, amongst others. The use of polygonal elements with $n-$ number of sides will provide greater flexibility and better accuracy to address some of these problems. Polygonal

finite element discretizations can be useful in many areas like, e.g. the nonlinear constitutive modeling of polycrystalline materials with general anisotropic or ferroelectric [1,2] behavior where each grain is represented with its independent properties by one element, for interface elements connecting dissimilar finite element meshes [3], for two field methods solving diffusion equations [4], for solid mechanics problems [5] including incompressible materials [6], and for topology optimization [7].

Methodology

Assume $\Omega \subset \mathbb{R}^2$ is a bounded convex domain with smooth boundary and $\mathcal{P}$ is a given set of distinct seeds in Ω. To construct a polygonal discretization of Ω, we first reflect all points in $\mathcal{P}$ about the closest boundary point of $\partial\Omega$ and denote the resulting set by $R_\Omega(\mathcal{P})$

$$R_\Omega(\mathcal{P}) = \{R_\Omega(\boldsymbol{P}_I) \colon (\boldsymbol{P}_I) \in (\mathcal{P})\} \tag{1}$$

Convexity of Ω ensures that all the reflected points lie outside Ω. We then construct the Voronoi diagram of the original point set as well as its reflection. In other words, we compute $\mathcal{V}(\mathcal{P} \cup R_\Omega(\mathcal{P}))$. If Voroni cells of a point $\boldsymbol{P}_I$ and its reflection have a common edge, i.e., if $\mathcal{V}(\boldsymbol{P}_I) \cap \mathcal{V}(R_\Omega(\boldsymbol{P}_I)) \neq \emptyset$, then this edge is tangent to $\partial\Omega$ at $\boldsymbol{P}_{b1}$ as in Fig.1. Therefore, these edges form an approximation to domain boundary and a reasonable discretization of Ω is given by the collection of Voronoi cells corresponding to the points in $\mathcal{P}$.

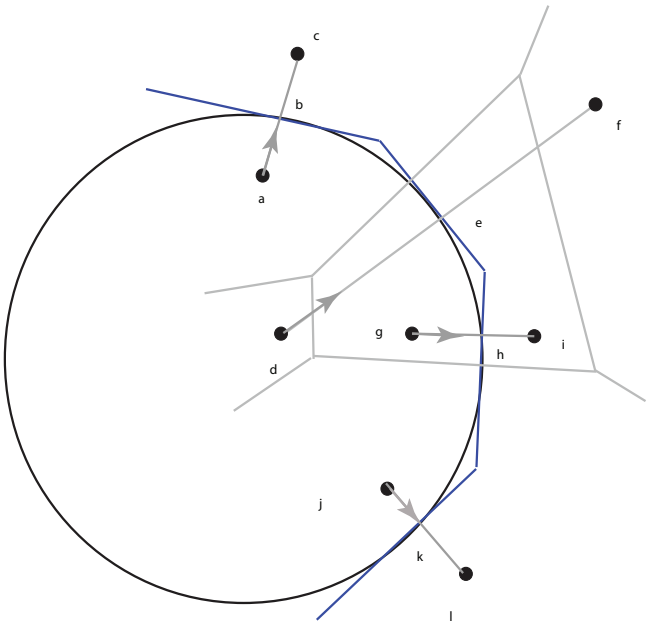

Figure 1: Voronoi edges shared between seeds and their reflection approximate the boundary of the domain. Reflection of interior seeds, say $\boldsymbol{P}_4$, has no effect on tracing the boundary of the domain.

Polygonal finite element discretization

In this section we present a simple and robust method for polygonal mesh generation. The main components of a mesh generator are an implicit description of the domain geometry and the centroidal Voronoi tessellation (CVT) used for its discretization. The signed distance function contains all the essential information about the domain geometry and offers great flexibility to construct a relatively large class of domains. Lloyd's method is used to ensure uniform (optimal) distribution of seeds and thus a high quality mesh [7].

Conforming interpolants on polygons

Though there are many interpolants defined over polygonal domains, we prefer to use the Laplace interpolant in our analysis owing to its ease and simplicity. Consider a set of $\mathcal{K}$ nodes $\boldsymbol{P}_I = (P_{Ix}, P_{Iy})$ in a domain $\Omega \in \mathbb{R}^2$. At any point $\boldsymbol{P} = (P_x, P_y)$ inside Ω or on its boundary $\partial\Omega$ a set of associated interpolants $\phi_I(\boldsymbol{P})$ is defined. Using this, an interpolation scheme for a scalar-valued function $f(\boldsymbol{P})$ can be written as

$$f^h(\boldsymbol{P}) = \sum_{I=1}^{N} \Phi_I(\boldsymbol{P}) f_I \tag{2}$$

where $f_I = f(\boldsymbol{P}_I)$ are the function values at the K nodes of the polygon. The function $\Phi_I(\boldsymbol{P})$, satisfies properties such as partition of unity, interpolation and linear completeness inside the polygon and on the boundaries. Various geometric measures like edge length, signed area, and sine or cosine of the angles at each vertex of the polygon are used to construct polygonal interpolants. The Laplace natural neighbor interpolant is the simplest and most popular Voronoi based interpolation method on polygonal domains. The scheme, originally based on the concept of natural neighbors is widely applicable for polygonal domains owing to its ease of implementation, and ability to account for a density distribution of nodes in a discretization. Fig.2 shows the Voronoi cells for an added point $\boldsymbol{P}$ within a (canonical) polygonal domain with six nodes.

The Laplace interpolation functions are defined using the geometric properties of the Voronoi cell as

$$\phi_I^{\mathrm{L}}(\boldsymbol{P}) = \frac{w_I(\boldsymbol{P})}{\sum_{J=1}^{N} w_J(\boldsymbol{P})} \tag{3}$$

$$w_I(\boldsymbol{P}) = \frac{s_I(\boldsymbol{P})}{h_I(\boldsymbol{P})} \tag{4}$$

where $s_I(\boldsymbol{P})$ is the length of the associated Voronoi edge and $h_I(\boldsymbol{P}) = \|\boldsymbol{P} - \boldsymbol{P}_I\|$ is the Euclidean distance from node $\boldsymbol{P}$ to node I, see Fig.2. As only lengths of the Voronoi cells are taken into account, this method belongs to the class of non-Sibsonian interpolants. The Laplace interpolant ϕ_I^{L}

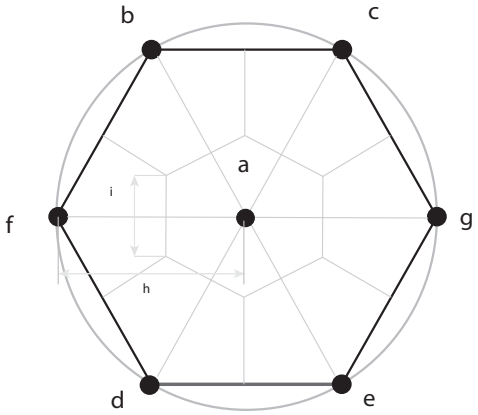

Figure 2: Voronoi based geometric measures for the Laplace interpolant: length of the associated Voronoi edge s_I, and the Euclidean distance h_I to the evaluation point $\boldsymbol{P}$.

on a canonical domain Ω_0, in which all nodes are regularly distributed on a unit circle, is shown in Fig.3.

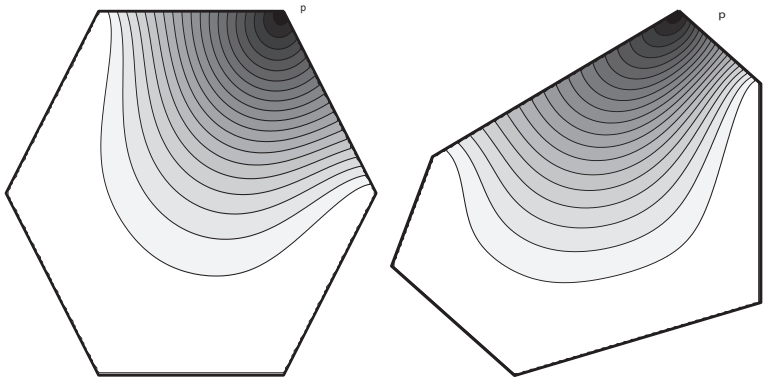

(a) (b)

Figure 3: Laplace interpolant ϕ_I^{L} on a) canonical hexagonal domain b) Physical polygonal domain .

Linear Elasticity : Governing equations and weak form

We consider the displacement field $\boldsymbol{u}(\boldsymbol{X})$ of a body described by an open bounded domain.

On the Dirichlet boundary Γ_u the displacements $\bar{u}_i$ are given, whereas the Neumann boundary Γ_σ is loaded by the prescribed surface forces $\bar{t}_i$. For small displacements, the governing equations are given by

$$\operatorname{div} \boldsymbol{\sigma} + \boldsymbol{b} = 0 \quad \text{in} \quad \Omega \tag{5a}$$

subjected to boundary conditions

$$\boldsymbol{u} = \bar{\boldsymbol{u}} \quad \text{on} \quad \Gamma_u \tag{5b}$$

$$\boldsymbol{t} = \boldsymbol{\sigma} \cdot \boldsymbol{n} = \bar{t}_i \quad \text{on} \quad \Gamma_\sigma \tag{5c}$$

with the body force per unit volume $\boldsymbol{b}$ and the unit outward normal $\boldsymbol{n}$ to Γ_σ.

The linear stress tensor follows from $\boldsymbol{\sigma} = \boldsymbol{D}\boldsymbol{\varepsilon}$ with the strain tensor $\boldsymbol{\varepsilon} = \frac{1}{2}[\nabla \boldsymbol{u} + \nabla^T \boldsymbol{u}]$ and the material moduli tensor $\boldsymbol{D}$. For a homogeneous isotropic material with the Navier-Lamé parameters λ and μ, we obtain

$$\boldsymbol{D} = \lambda \mathbf{1} \otimes \mathbf{1} + 2\mu \boldsymbol{I}. \tag{6}$$

Where $\mathbf{1}$ is a second order identity tensor. and $\boldsymbol{I}$ is a symmetric fourth order identity tensor. The weak form is consequently expressed as

$$\int_\Omega \boldsymbol{\sigma}(\boldsymbol{u}) : \boldsymbol{\varepsilon}(\boldsymbol{\eta})\, d\Omega = \int_\Omega \boldsymbol{b} \cdot \boldsymbol{\eta}\, d\Omega + \int_\Gamma \bar{\boldsymbol{t}} \cdot \boldsymbol{\eta}\, d\Gamma. \tag{7}$$

For the discretization a displacement trial solution of the form $u_i^h \in V = [H^1(\Omega)]^2$ is chosen together with a set of kinematically admissible test functions $\eta_i^h \in V_0 = [H_0^1(\Omega)]^2$, vanishing on the Dirichlet boundaries. The trial and test functions are represented as linear combinations of C^0 continuous interpolation functions,

$$\boldsymbol{u}^h(\boldsymbol{X}) = \sum_{I=1}^{N} \phi_I(\boldsymbol{X}) \boldsymbol{u}_I \quad \text{and} \quad \boldsymbol{\eta}^h(\boldsymbol{X}) = \sum_{I=1}^{N} \phi_I(\boldsymbol{X}) \boldsymbol{\eta}_I, \tag{8}$$

On substituting the trial and test functions and using the arbitrariness of nodal variations, the discrete system of linear equations

$$\boldsymbol{K}\boldsymbol{u} = \boldsymbol{f} \tag{9}$$

is obtained with the stiffness matrix

$$\boldsymbol{K} = \int_{\Omega^h} \boldsymbol{B}^T \boldsymbol{D} \boldsymbol{B}\, d\Omega^h \tag{10}$$

and the external load vector

$$\boldsymbol{f} = \int_{\Gamma^h} \boldsymbol{\phi} \bar{\boldsymbol{t}}\, d\Gamma^h + \int_{\Omega^h} \boldsymbol{\phi} \boldsymbol{b}\, d\Omega^h \tag{11}$$

where the matrix of the shape function derivatives is given by

$$\boldsymbol{B} = \begin{bmatrix} \boldsymbol{\phi}_{I,X} & 0 \\ 0 & \boldsymbol{\phi}_{I,Y} \\ \boldsymbol{\phi}_{I,Y} & \boldsymbol{\phi}_{I,X} \end{bmatrix}$$

and the material moduli tensor in Voigt notation for an isotropic linear material and plane stress condition is given by

$$\boldsymbol{D} = \frac{E}{1-\nu^2}\begin{bmatrix} 1 & \nu & 0 \\ \nu & 1 & 0 \\ 0 & 0 & \frac{1-\nu}{2} \end{bmatrix}$$

Numerical Example

In this section, We consider an example under plane stress conditions to demonstrate the proposed method. Numerical integration on an $n-$ sided polygon is performed using 3×3 Gauss quadrature rule on $n-$ sub - triangles of a n sided polygon. In the example considered we use modulus of elasticity $E = 70000$ Mpa and Poisson's ratio, $\nu = 0.3$.

Plate with a Circular hole

A non - convex plate with a traction - free circular hole is considered (edge length 2ℓ, hole radius $a = \frac{\ell}{6}$). Fig.4 shows the quarter plate loaded by unidirectional tension $\sigma_0 = 100$ Mpa in X - direction on the right edge. Due to symmetry, Dirchlet boundary conditions are imposed along $AB(u_y = 0)$ and $DE(u_x = 0)$. The corresponding displacement components are

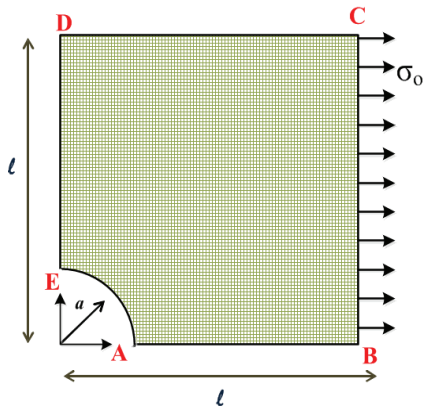

Figure 4: Quarter plate with circular hole under tension with symmetry axes

$$\begin{aligned} u_x(r,\theta) &= \frac{a}{8\mu}\left[\frac{r}{a}(\kappa+1)\cos\theta + 2\frac{a}{r}((1+\kappa)\cos\theta \right. \\ &\qquad \left. + \cos 3\theta) - 2\frac{a^3}{r^3}\cos 3\theta\right] \qquad (12) \\ u_y(r,\theta) &= \frac{a}{8\mu}\left[\frac{r}{a}(\kappa-3)\sin\theta + 2\frac{a}{r}((1-\kappa)\sin\theta \right. \\ &\qquad \left. + \sin 3\theta) - 2\frac{a^3}{r^3}\sin 3\theta\right] \qquad (13) \end{aligned}$$

with $\kappa = 3-4\nu$. In the numerical computations, we consider $a = 10mm$, $\ell = 60mm$ and the Laplace interpolant ϕ_I^{L}. As a termination criteria we have chosen $\eta_{all} = 5\%$.

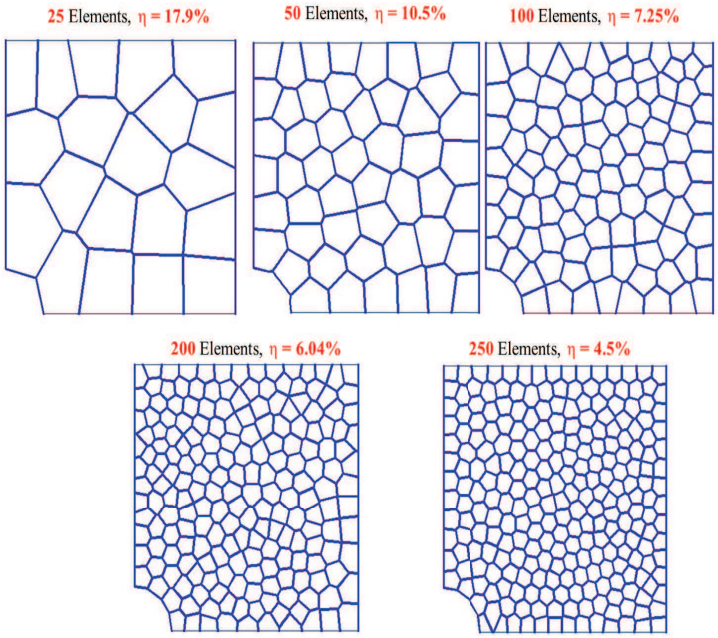

Figure 5: Meshes generated due to uniform refinement of the plate with a circular hole domain

Initial discretization being the coarsest has 25 elements with 104 degrees of freedom. Following the procedure described earlier we perform an uniform and adaptive refinement on this initial coarse mesh. Fig.5 shows the different meshes obtained due to uniform refinement.

We see that adaptive refinement converges at a relatively higher rate than uniform refinement. The stress plots for the plate with a hole example are shown in Fig.6.

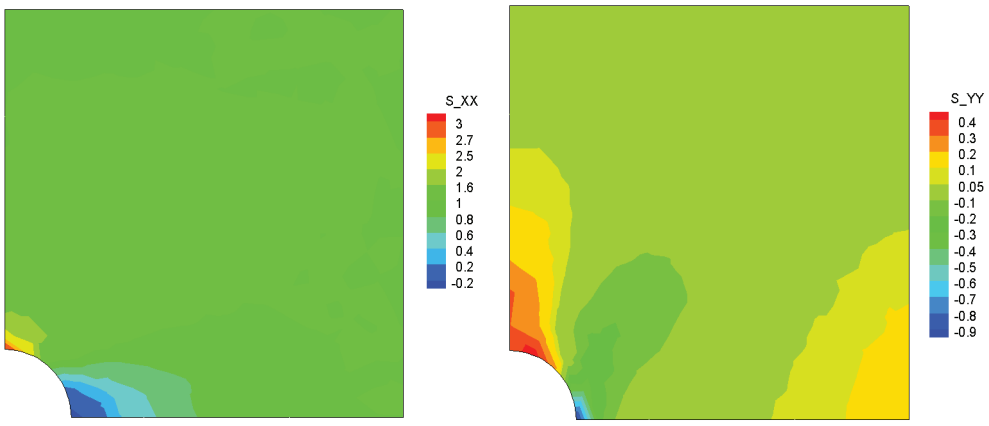

(a) (b)

Figure 6: Stress plot for plate with a circular hole problem on the finest adaptive refined mesh. (a)σ_{xx} (b)σ_{yy}

References

1)K. Y. Sze and N. Sheng, Polygonal finite element method for nonlinear constitutive modeling of polycrystalline ferroelectrics, Finite Elements in Analysis and Design, 42, 107-129, (2005).

2)A. Jayabal, K. Menzel and A. Arockiarajan, Micromechanical modelling of switching phenomena in polycrystalline piezoceramics: application of polygonal finite element approach, Computational Mechanics, 48, 421-435, (2011).

3) C. R. Dohrmann, W. K. Samuel, and M. W. Heinstein, A method for connecting dissimilar finite element meshes in two dimensions, International Journal for Numerical Methods in Engineering, 48, 655-678, (2000).

4) Y. A. Kuznetsov, Mixed finite element method for diffusion equations on polygonal meshes with mixed cells, Journal of Numerical Mathematics, 14, 305-315, (2006).

5) M. M. Rashid and P. M. Gullett, On a finite element method with variable element topology, Computational Methods in Applied Mechanics and Engineering, 190, 1509-1527, (2000).

6) K. Y. Dai, G. R. Liu, and T. T. Nguyen, An n-sided polygonal smoothed finite element method (nSFEM) for solid mechanics, Finite Elements in Analysis and Design, 43, 847-860, (2007).

7) C. Talischi, G. Paulino, A. Pereira, and I. Menezes, Polygonal finite elements for topology optimization: A unifying paradigm, International Journal for Numerical Methods in Engineering, 82, 671-698, (2010).